Available online at www.sciencedirect.com
ScienceDirect
Journal of Nuclear Materials 373 (2008) 217–225
journal of nuclear materials
www.elsevier.com/locate/jnucmat

Evidence for basal $\langle a \rangle$-slip in Zircaloy-2 at room temperature from polycrystalline modeling

F. Xu *, R.A. Holt, M.R. Daymond

Department of Mechanical and Materials Engineering, Queen's University, Kingston, Ontario, Canada K7L 3N6

Received 5 December 2006; accepted 16 May 2007

Abstract

Polycrystalline modeling has been used to interpret the evolution of lattice strain and texture in zirconium based alloys. Challenges in matching model and experimental results have mainly arisen from an insufficient knowledge of intrinsic deformation mechanisms (slip and twinning). Specifically, there is little concrete evidence that basal $\langle a \rangle$-slip occurs during room-temperature deformation or whether pyramidal $\langle a \rangle$-slip is an alternate mechanism. Also, the critical resolved shear stresses (CRSSs) for slip and twinning systems relevant to polycrystals are not well established. We have developed an understanding of the contribution of basal $\langle a \rangle$-slip to deformation by applying an elasto-plastic self-consistent model to an extensive experimental database, obtained by neutron diffraction measurements on textured Zircaloy-2. By considering a variety of slip system combinations, the roles of each slip system in lattice strain development were investigated. Parameters for the model were obtained by best fitting to a large experimental database, including both macroscopic data (flow curves and Lankford coefficients) and microscopic internal strain data. Based on optimized agreement between model and experimental data we conclude that there is evidence that basal slip does occur, while the effects which might be attributed to pyramidal $\langle a \rangle$-slip can be represented by the influence of other combinations of slip systems. We propose reasonable ranges of initial CRSSs for each slip system, which should benefit the modeling of similar materials (e.g. Zircaloy-4).

1. Introduction

Zirconium and its alloys are characterized by pronounced mechanical anisotropy, which originates from the anisotropic single crystal *hcp* structure and bulk crystallographic texture. This anisotropy is manifest in the thermal expansion coefficients, elastic modulae, and plastic properties, i.e. different critical resolved shear stresses (CRSS), and hardening behavior for different slip and twinning systems. The plastic deformation mechanisms observed in Zr and its various alloys [1] include slip in $\langle a \rangle$-direction: $\{10\bar{1}0\}\langle 11\bar{2}0\rangle$ prism slip (pr), $\{0001\}\langle 11\bar{2}0\rangle$ basal slip (bas) and $\{10\bar{1}1\}\langle 11\bar{2}0\rangle$ pyramidal slip (pya); slip in $\langle c+a \rangle$-direction: $\{10\bar{1}1\}\langle 11\bar{2}3\rangle$ first-order pyramidal slip (pyca) and $\{11\bar{2}1\}\langle 11\bar{2}3\rangle$ second-order pyramidal slip; tensile twinning: $\{10\bar{1}2\}\langle 10\bar{1}1\rangle$ (tt) and $\{11\bar{2}1\}\langle 11\bar{2}6\rangle$; and compressive twinning: $\{11\bar{2}2\}\langle 11\bar{2}3\rangle$ and $\{10\bar{1}1\}\langle 10\bar{1}2\rangle$. Prism slip is the most easily activated (i.e. has the lowest CRSS) and is always present when a polycrystal is deformed regardless of deformation conditions. Other deformation systems are activated only under specific circumstances, i.e. combinations of temperature and stress sense relative to the bulk texture. For example, tensile twinning is activated only when the $\langle c \rangle$-axis of a particular crystal is placed under tension.

There is general agreement in the literature that deformation of Zr and its alloys at room temperature is accommodated by prism $\langle a \rangle$-slip, first-order pyramidal $\langle c+a \rangle$-slip and $\{10\bar{1}2\}\langle 10\bar{1}1\rangle$ tensile twinning. The experimental evidence, derived from single-trace methods [2] or transmission electron microscopy (TEM) observations, has been well documented for the presence of prism slip [3–5] and pyramidal $\langle c+a \rangle$-slip [6–8], as well as tensile twinning [4,9,10]. Prism slip always activates first with

* Corresponding author. Fax: +1 613 533 6610.
E-mail address: holt@me.queensu.ca (F. Xu).

0022-3115/$ - see front matter © 2007 Elsevier B.V. All rights reserved.
doi:10.1016/j.jnucmat.2007.05.052

increasing applied stress. As a higher stress is applied, the $\langle a \rangle$ dislocations accumulate, forming local stress concentrations where it is possible for cross-slip to operate. Cross-slip of the $\langle a \rangle$ dislocations is a likely mechanism for the initiation of basal slip and/or pyramidal $\langle a \rangle$-slip. However, there is little conclusive experimental evidence of the presence of these two slip systems to date, principally due to the difficulty in unambiguously identifying the slip plane by TEM observations. Slip markings belonging to (or close to) basal traces have been discovered in (1) single crystal Zr (99.8–99.9 wt%) in regions of stress concentration at room temperature [11], (2) single crystal Zr at elevated temperatures [12], (3) commercial grade Zr near hydride particles [5], (4) irradiated Zircaloy [13] and (5) polycrystal Zr at elevated temperatures during kink formation [14]. In brief, there is no direct evidence for basal slip in polycrystal Zr alloys at room temperature, but there is evidence for basal slip under other circumstances. To the best of our knowledge, there is no published evidence for pyramidal $\langle a \rangle$-slip under any circumstances (the paper cited in Ref. [15] was not published).

The inclusion of basal slip in the polycrystalline modeling (e.g. elasto-plastic [16] and visco-plastic self-consistent [17] models) has been found to improve the ability to reproduce experimental macroscopic flow curves [18] and bulk texture development [19–21] caused by plastic deformation. However, other researchers [15,22–24] have instead preferred to include pyramidal $\langle a \rangle$-slip as an alternative to basal slip in order to achieve optimal agreement with their experimental data.

The lack of sufficient knowledge regarding values of CRSSs appropriate for deformation systems also constitutes a difficulty for performing polycrystalline modeling. Practically, CRSSs must be derived indirectly through polycrystalline modeling using an 'inverse approach' [25], since the manufacture of single crystals of many alloys to allow measurement of the CRSSs is either very difficult or in some cases impossible. Further, the observed CRSSs required for model fitting in a polycrystal will be different from those found in a single crystal due to the interactions of the dislocations with grain boundaries.

In this paper we aim to provide a better understanding of the influence of basal slip and its contribution to polycrystalline plasticity. Through *in situ* tension and compression tests in neutron spectometers, we have obtained an extensive experimental data set of both flow curves and internal lattice strain development along the three principal directions of a textured Zircaloy-2 slab. These data are reported in full in Ref. [26]. This data set represents a far more extensive data set than that available elsewhere in the literature, and hence a more exacting test of polycrystal models.

This paper considers a variety of combinations of deformation systems, using a previously published elasto-plastic self-consistent model (EPSC [16]). The model results are compared to the experimental flow curves, the Lankford coefficients (also referred to as R values), and internal lattice strain development. In particular, we illustrate the influence of basal slip. Reasonable ranges of CRSSs for the commonly selected slip systems are also provided, which may be helpful for the modeling of similar materials (e.g. Zircaloy-4).

2. Background

2.1. Neutron diffraction measurements

We performed the *in situ* neutron diffraction measurements at different sites, using the time-of-flight technique for the compression tests at the ISIS neutron source, Rutherford Appleton Laboratory, UK, and using the constant-wavelength technique for the tensile tests at NRU reactor, Chalk River Laboratories, Canada. We have corrected the tensile test data to a strain rate equivalent to that used in the compression tests [26], for the purpose of direct comparisons. The experimental set-up for each of the neutron diffraction techniques is described in Refs. [27,18]. For the time-of-flight measurement, the sample is placed horizontally at 45° to the (horizontal) incident white beam, with two detector banks sitting at scattering angles of $\pm 90°$. This allows a concurrent measurement of lattice spacings in the loading direction and one of the two Poisson directions. Two tests are needed to obtain the lattice strain development in three principal directions. In a constant-wavelength test, only one detector is used. The sample is positioned so that the scattering vector is parallel to either the loading direction or either of the two Poisson directions. Three samples are needed for a three-dimensional lattice strain measurement. In a neutron measurement, an 'orientation' comprises a family of grains with a particular plane normals lying within a few degrees off the nominal orientation (roughly $\pm 6.5°$ at ISIS and $\pm 0.5°$ at NRU) corresponding to the crystals contributing to one measurement. Note that the measured lattice strain is the average lattice strain for an 'orientation'.

2.2. Elasto-plastic self-consistent model

The EPSC model is an Eshelby equivalent inclusion model, which deals with interactions between Eshelby inclusions and an infinite homogeneous effective medium (HEM) that is subjected to an external load. Each inclusion represents a particular grain orientation. The inclusions, the HEM and the interactions between them are both elastically and plastically anisotropic and the properties of the HEM are the weighted average properties of all the inclusions. A solution is obtained by iteration until the response of the HEM correctly represents the overall response of the polycrystal. The polycrystal can be textured, with grain populations being grouped into different families according to their orientations. A more detailed description of the model can be found elsewhere [16].

The model generates the macroscopic flow history, and as well, it produces the lattice strain evolution for each

'orientation'. These can be averaged for a specified family of grains corresponding to the 'orientations' for which the lattice strains are measured by neutron diffraction. This allows direct comparison with neutron diffraction data. In addition, the model offers insights on the relative activities of individual deformation modes and the absolute average activity of all the slip and twinning systems. The model has been applied to a wide variety of materials of *fcc* (e.g. [27,28]), and also *hcp* (e.g. [29,30]) structures when twinning does not make a significant contribution.

In each grain orientation, the individual deformation mode (including both slip and twinning) is assigned with an initial CRSS, which develops as the deformation proceeds. This hardening behavior (i.e. the development of CRSS) of each deformation mode s is represented by an extended empirical Voce hardening expression [31]:

$$\tau^s = \tau_0^s + (\tau_1^s + \theta_1^s \Gamma)[1 - \exp(-\theta_0^s \Gamma/\tau_1^s)], \quad (1)$$

where τ^s is the instantaneous CRSS, τ_0^s and $\tau_0^s + \tau_1^s$ are the initial and final back-extrapolated CRSS, respectively. θ_0^s and θ_1^s are the initial and asymptotic hardening rates, and Γ is the accumulated plastic shear in the grain. The model also allows for the possibility of 'self' and 'latent' hardening by defining coupling coefficients $h^{s/s'}$ which empirically account for the obstacles to deformation the mode s' represent for deformation of mode s [31]:

$$\Delta\tau^s = \frac{d\tau^s}{d\Gamma} \sum_{s'} h^{s/s'} \Delta\gamma^{s'}. \quad (2)$$

2.3. Major findings in the related previous work

In Ref. [32], we demonstrated that a moderately strong bulk texture led to very different deformation mechanisms operating dependent on the sense of the applied loading. We found that tensile twinning occurs in specimens deformed in tension along the normal direction (Tens.ND), or in compression along the rolling direction (Comp.RD) and transverse direction (Comp.TD) of the slab, while twinning is negligible in the other three deformation conditions, i.e. compression along the normal direction (Comp.ND) or tension along the rolling direction (Tens.RD) and transverse direction (Tens.TD).

Based on the majority, but not all of the literature, in the model used in Ref. [32] we considered prism $\langle a \rangle$-slip, basal $\langle a \rangle$-slip, first-order pyramidal $\langle c + a \rangle$-slip and tensile twinning, and based on this assumption we found optimum agreement between model and experiment. In Tens.TD and Tens.RD, prism slip was the dominant mode, while pyramidal $\langle c + a \rangle$-slip operated to a negligible extent, with basal slip operating at an intermediate level. In contrast, in Comp.ND, basal slip and pyramidal $\langle c + a \rangle$-slip were highly active. The intensity changes of the measured diffraction peaks in Comp.ND were rather subtle, suggesting that the texture changes are insignificant under this loading condition. However, the intensity of prism orientations in Tens.TD and Tens.RD changed rather dramatically, providing a strong indication of texture change [33].

In the model [32] we also considered the influence of latent hardening (i.e. hardening due to slip system interactions). It was found that latent hardening has potent effects not only on the lattice strain calculations, but also on the predicted Lankford coefficients, especially in the cases of Comp.RD and Comp.TD (but not in Comp.ND).

3. Modeling procedure

In this paper, we have used the same EPSC model applied in Ref. [32] to further interpret the experimental flow curves and lattice strain evolution, with the goal of exploring the relative contributions of different combinations of slip systems in matching the observed experimental data. Texture measurements [34] indicated that in the Zircaloy-2 slab (from which tension and compression specimens were prepared), most basal grains are initially oriented towards ND, with a few towards TD and very few towards RD. We represent the measured slab texture using a population of 1944 suitably weighted grains as described in Ref. [32]. The principal difference between the modeling work described in Ref. [32] and here, is that in this work the latent hardening (i.e. hardening due to slip system interactions) is not considered for simplicity, since our earlier modeling has shown that latent hardening has only a marginal influence on the calculated lattice strains and R values for Comp.ND. Comp.ND is also the only loading condition we explored in which neither twinning of any type nor much texture development was observed.

To illustrate the roles of basal and pyramidal $\langle a \rangle$-slip on lattice strain evolution, we consider five cases with different slip system combinations (Table 1). The purpose of considering Case IV (which is not physically realistic, since prism slip is absent) is to display the effects of prism slip by comparison with Cases III and V. Case VI is the combination used in Ref. [32] that demonstrates the effect of tensile twinning.

In each of the five cases (I–V), we derive initial CRSS and Voce hardening parameters (i.e. τ_0 and θ_0; linear hardening is selected for simplicity, thus τ_1=0 and $\theta_0 = \theta_1$) for each slip system in an approach described as follows.

First, we define the criteria used to test the suitability of the parameters used in the EPSC model. On the macroscopic scale, we require that modeling results should

Table 1
Modeling cases of deformation system combinations

Case	Prism $\langle a \rangle$-slip	Basal $\langle a \rangle$-slip	Pyr. $\langle a \rangle$-slip	Pyr. $\langle c + a \rangle$-slip	Tensile twin
I	√			√	
II	√		√	√	
III	√	√		√	
IV		√	√	√	
V	√	√	√	√	
VI [32]	√	√		√	√

Table 2
Critical resolved shear stresses [GPa] and Voce hardening parameters used in modeling

	Case I		Case II		Case III		Case IV		Case V		Case VI	
	τ_0	θ_0	τ_0	θ_0	τ_0	θ_0	τ_0	θ_0	τ_0	θ_0	τ_0	θ_0
Prism $\langle a\rangle$-slip	0.08	0.001	0.08	0.01	0.10	0.06	–	–	0.10	0.06	0.10	0.02
Basal $\langle a\rangle$-slip	–	–	–	–	0.16	0.001	0.17	0.001	0.15	0.001	0.16	0.02
Pyr. $\langle a\rangle$-slip	–	–	0.12	0.01	–	–	0.12	0.05	0.14	0.05	–	–
Pyr. $\langle c+a\rangle$-slip	0.18	0.80	0.32	0.60	0.32	0.80	0.34	0.80	0.33	0.80	0.32	0.40
Tensile twin.	–	–	–	–	–	–	–	–	–	–	0.24	0.10

simultaneously capture the macroscopic responses (flow curves and Lankford coefficients) for Comp.ND, Tens.TD and Tens.RD, during which twinning is negligible. On the microscopic scale, the results should capture the experimental lattice strain evolution during Comp.ND, both parallel and perpendicular to the applied load (i.e. three measured data sets). One reason of choosing only the Comp.ND data set is because the EPSC model (a) does not account for significant texture evolution (which was observed in Tens.TD and Tens.RD) and has limited capabilities in dealing with twinning induced stress relaxation (which was observed in the remaining data sets). Another reason is that in Comp.ND secondary slip (slip other than the prism slip) is much more active compared to that in the loading along TD or RD, since only a few orientations are favorably deformed by prism slip.

Second, compared to the values used in our previous work [32] and reported in the literature we have set a wide exploratory range of initial CRSSs (τ_0) for each slip system in order to ensure we are not overlooking any reasonable parameter combinations. This approach means that we are exploring a much wider parameter space than would be considered by, for example, simply starting with 'good estimates' and carrying out a least-squares optimization. The ranges considered in this paper are as follows (in GPa): $0.06\leqslant \tau_0^{pr} \leqslant 0.16$, $0.05\leqslant \tau_0^{bas} \leqslant 0.35$, $0.05\leqslant \tau_0^{pya} \leqslant 0.35$ and $0.10\leqslant \tau_0^{pyca} \leqslant 0.40$.

Finally, we construct a large orthogonal 'grid' of CRSS combination within the set ranges, with an initial step of 0.05 GPa for each slip system. The result obtained using the input parameters for each 'grid point' is then tested for agreement with the experimental data sets. Those 'grid points' resulting in reasonable agreement with experiments are then selected as the starting points for the next round of 'optimization', at which a finer step of 0.01 GPa is applied, and a new grid of data points is obtained. The 'best fit' parameter combinations determined by this method are, shown in Table 2.

4. Modeling results

4.1. Macroscopic behavior

The calculated macroscopic flow curves for each of the five cases are depicted in Fig. 1, superimposed on their experimental counterparts. For most cases the agreement between the model and experiment is reasonable, with the exception of Cases I and IV where no basal slip or prism slip is considered. Table 3 tabulates experimental and calculated Lankford coefficients, which are defined as the ratio of contractions (or expansions) in two Poisson directions after a specimen is pulled (or compressed). The comparison shows good agreement with experiment if basal slip is included (Cases III, IV and V); without it (Cases I and II) the R values are too high to be correct for Tens.TD and Tens.RD. This is generally understood by considering the initial texture and Schmid factors. Schmid factors are highest for basal slip in the high-order pyramidal orientations ($\{10\bar{1}2\}$, $\{10\bar{1}3\}$ and $\{11\bar{2}2\}$), most of which are initially orientated close to ND. Thus basal slip can effect substantial deformation along ND (the plastically hardest direction), resulting in lower R values compared to the

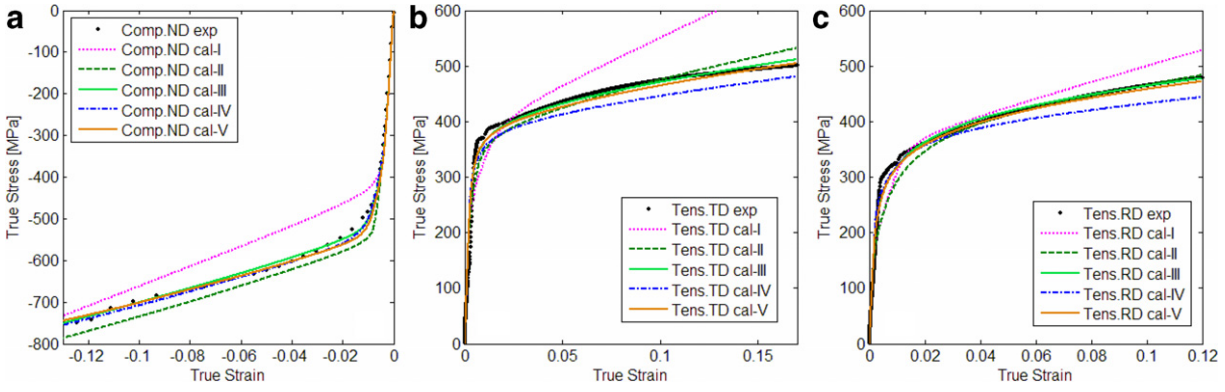

Fig. 1. Experimental and predicted flow curves for: (a) compression along ND, (b) tension along TD and (c) tension along RD.

Table 3
Experimental and calculated Lankford coefficients

	Experimental	Case I	Case II	Case III	Case IV	Case V
Comp.ND	1.01	2.94	1.69	1.15	1.10	1.22
Tens. TD	3.46	7.93	5.15	2.99	2.91	3.44
Tens. RD	2.61	3.00	3.94	2.60	3.23	3.08

cases where no basal slip is included during tension along RD and TD. This is clearer in tension along TD, where the two Poisson directions are the 'softest' (RD) and the 'hardest' (ND).

The insignificant differences in calculated flow curves and R values across Cases III–V reflect the fact that reproducing only the macroscopic behavior is not sufficient to reveal intrinsic deformation mechanisms microscopically.

4.2. Lattice strain development

We compare the predicted lattice strain development using different combinations of slip systems (Cases I–V) to the experimental data in three directions, which were obtained during compression along ND. We will omit the lattice strain data for some of the diffraction peaks for brevity (one should note that, in doing this, none of the measured peaks was actually overlooked): (1) $\{11\bar{2}0\}$ and $\{20\bar{2}1\}$ (similar to that for $\{10\bar{1}0\}$) in all the three directions, (2) $\{11\bar{2}2\}$ in ND and TD (similar to that for $\{10\bar{1}1\}$) and (3) $\{0002\}$, $\{10\bar{1}3\}$ and $\{10\bar{1}2\}$ in RD (for their low intensity and resultant large experimental errors).

4.2.1. Case I

In Case I ('pr+pyca'), the general trend of lattice strains of the low-order peaks (e.g. $\{10\bar{1}0\}$, $\{11\bar{2}0\}$ and $\{20\bar{2}1\}$) in the loading direction (Fig. 2(a)) is roughly acceptable. This suggests that the CRSS of prism slip and its hardening are within reasonable ranges, as the yielding and hardening of the low-order orientations are mainly controlled by prism slip (Schmid factor is high). For other pyramidal orientations and the basal orientation, the agreement between the model and experiment is unacceptable. In the two Poisson directions (Fig. 2(b) and (c)), it is obvious that even the general trend in the lattice strain development is missed for all the plotted diffraction peaks. This poor agreement cannot be improved by simply tuning the model parameters (within the ranges given in Section 3). Thus we infer that considering only prism $\langle a\rangle$-slip and pyramidal $\langle c+a\rangle$-slip is not sufficient to reproduce the experimental lattice strain data.

4.2.2. Case II

In Case II ('pr+pya+pyca'), predicted lattice strains in the loading direction (Fig. 3(a)) are acceptable. In particular, the difference between $\{10\bar{1}1\}$ and $\{10\bar{1}2\}$ lattice strains in the plastic regime is captured by the model, which was not successfully reproduced in our previous work [32]. However, the model fails to reproduce the lattice strain development for all the diffraction peaks in the Poisson directions (Fig. 3(b) and (c)). Again, simply adjusting the model parameters does not help improve the agreement.

4.2.3. Case III

If we replace pyramidal $\langle a\rangle$-slip with basal slip (Case III, 'pr+bas+pyca'), the agreement between the model and experiment in the two Poisson directions is much improved (Fig. 4(b) and (c)), compared to Cases I and II. However, it is noted that the predicted $\{0002\}$ strain in TD still deviates from the experimental data during plastic deformation, as in the previous two cases. This deviation is induced by the exclusion (on purpose) of tensile twinning in modeling, which, although negligible, has a strong effect in reproducing the basal strain in TD. This will be clearer when comparing Cases III and VI [32]. The higher yield strength shown in Fig. 4(b) than that in Fig. 4(a) and (c) is due to the texture variation in the two specimens [26] used for the compression testing along ND. In the loading

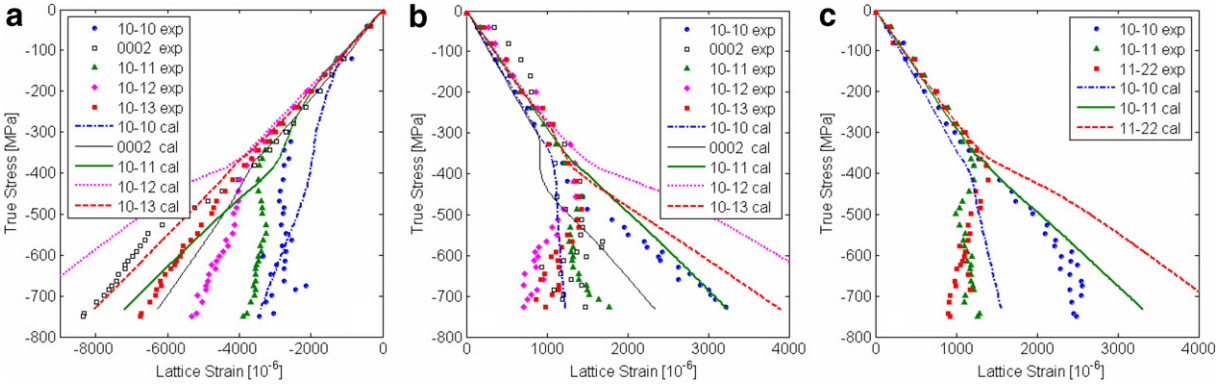

Fig. 2. Predicted and measured 3-D lattice strain evolution during compression along ND, Case I: (a) lattice strains along ND, (b) lattice strains along TD and (c) lattice strains along RD. The sample was tested such that $Q_1\|$ND (a) and $Q_2\|$TD (b) or $Q_1\|$ND and $Q_2\|$RD (c).

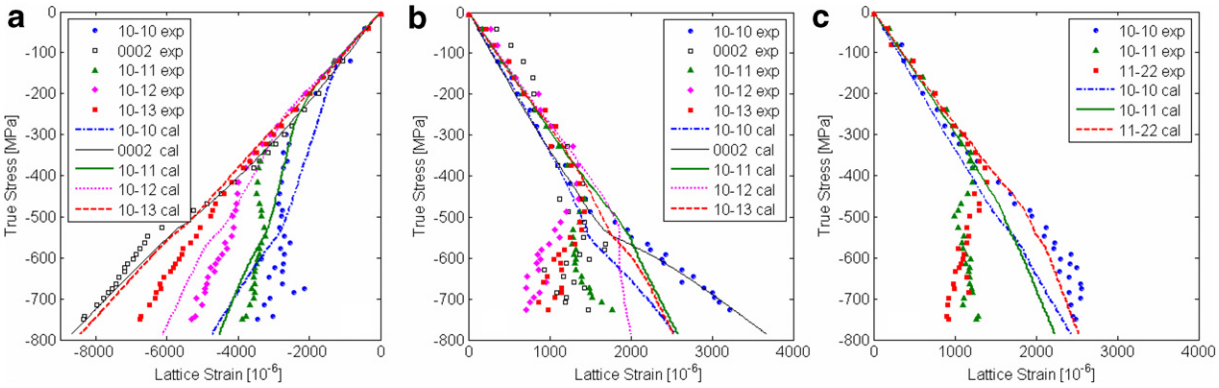

Fig. 3. Predicted and measured 3-D lattice strain evolution during compression along ND, Case II: (a) lattice strains along ND, (b) lattice strains along TD and (c) lattice strains along RD.

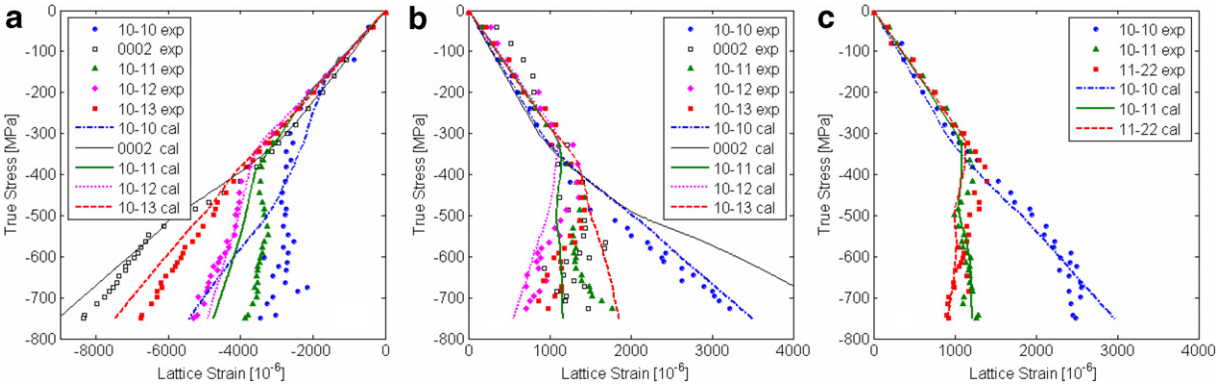

Fig. 4. Predicted and measured 3-D lattice strain evolution during compression along ND, Case III: (a) lattice strains along ND, (b) lattice strains along TD and (c) lattice strains along RD.

direction (Fig. 4(a)), the model results are acceptable, but the difference between $\{10\bar{1}1\}$ and $\{10\bar{1}2\}$ strains is hard to discern. As shown in Case III, basal slip brings about micro-yielding [26] of the high-order pyramidal orientations: this is consistent with the relatively high Schmid factors in these orientations. Once these pyramidal orientations yield, load is transferred to the lower-order grains, such as $\{10\bar{1}0\}$, $\{11\bar{2}0\}$, $\{20\bar{2}1\}$ and $\{10\bar{1}1\}$, and thus their lattice strains keep increasing. Case III shows that basal slip is necessary in the modeling.

4.2.4. Case IV

Case IV ('bas+pya+pyca') is unrealistic and was only designed to illustrate the effects of prism and pyramidal $\langle a\rangle$-slip. Fig. 5 clearly shows that the lattice strain development in all the three directions is not much different from that in Case III, except for prism orientations (e.g. $\{10\bar{1}0\}$) in the loading direction, and $\{11\bar{2}2\}$ in RD. Two points are apparent. First, without prism slip, the micro-yielding of the prism grains cannot be reproduced (even using other model parameters), resulting in rapidly

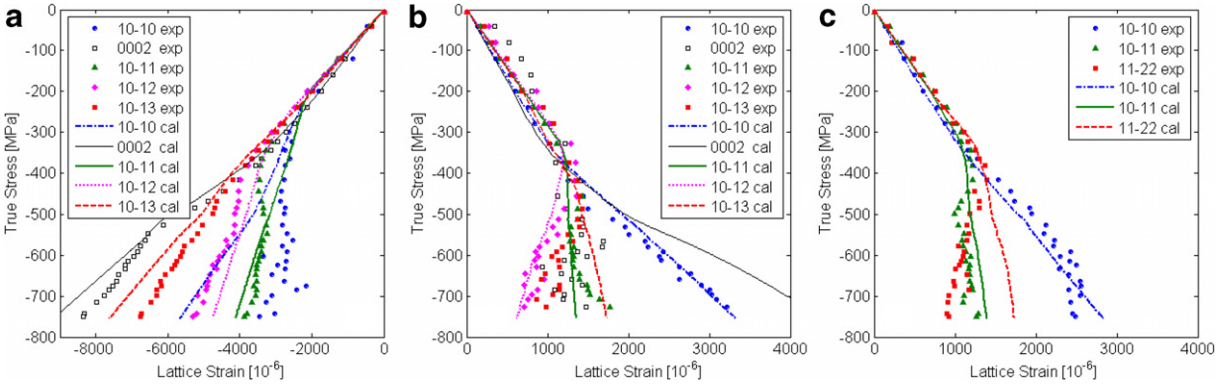

Fig. 5. Predicted and measured 3-D lattice strain evolution during compression along ND, Case IV: (a) lattice strains along ND, (b) lattice strains along TD and (c) lattice strains along RD.

increasing lattice strains in these grains during plastic deformation. Therefore prism slip should not be ignored, and cannot be substituted by pyramidal ⟨*a*⟩-slip. Secondly, pyramidal ⟨*a*⟩-slip is not an essential deformation mode for modeling, since without it the lattice strains (especially those of pyramidal grains) still can be reproduced as shown in Case III.

4.2.5. Case V

In Case V ('pr+bas+pya+pyca') all the commonly used slip systems are considered. More parameters are needed to be tuned, and thus more effort was spent compared to the previous four cases. However, this effort does not lead to noticeably better agreement than Case III in all the three directions (Fig. 6), except that the separation of $\{10\bar{1}1\}$ and $\{10\bar{1}2\}$ strains is a little improved in the loading direction. It is then deduced, again, that pyramidal ⟨*a*⟩-slip is not indispensable for modeling; its effect can be represented by other slip systems.

4.3. Relative activities of slip systems

Fig. 7 presents how the slip systems compete with each other during deformation in each of the five cases, based on which, a clearer understanding of basal and pyramidal ⟨*a*⟩-slip is apparent. It is shown that prism slip (or

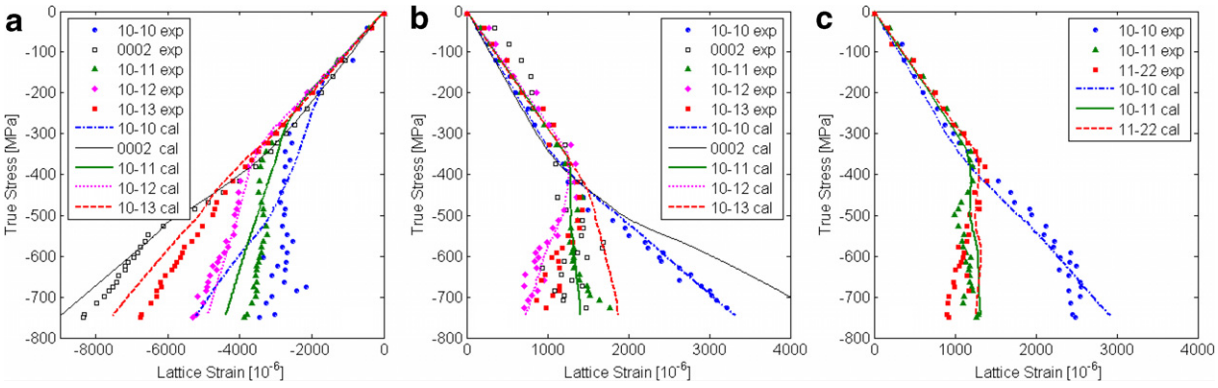

Fig. 6. Predicted and measured 3-D lattice strain evolution during compression along ND, Case V: (a) lattice strains along ND, (b) lattice strains along TD and (c) lattice strains along RD.

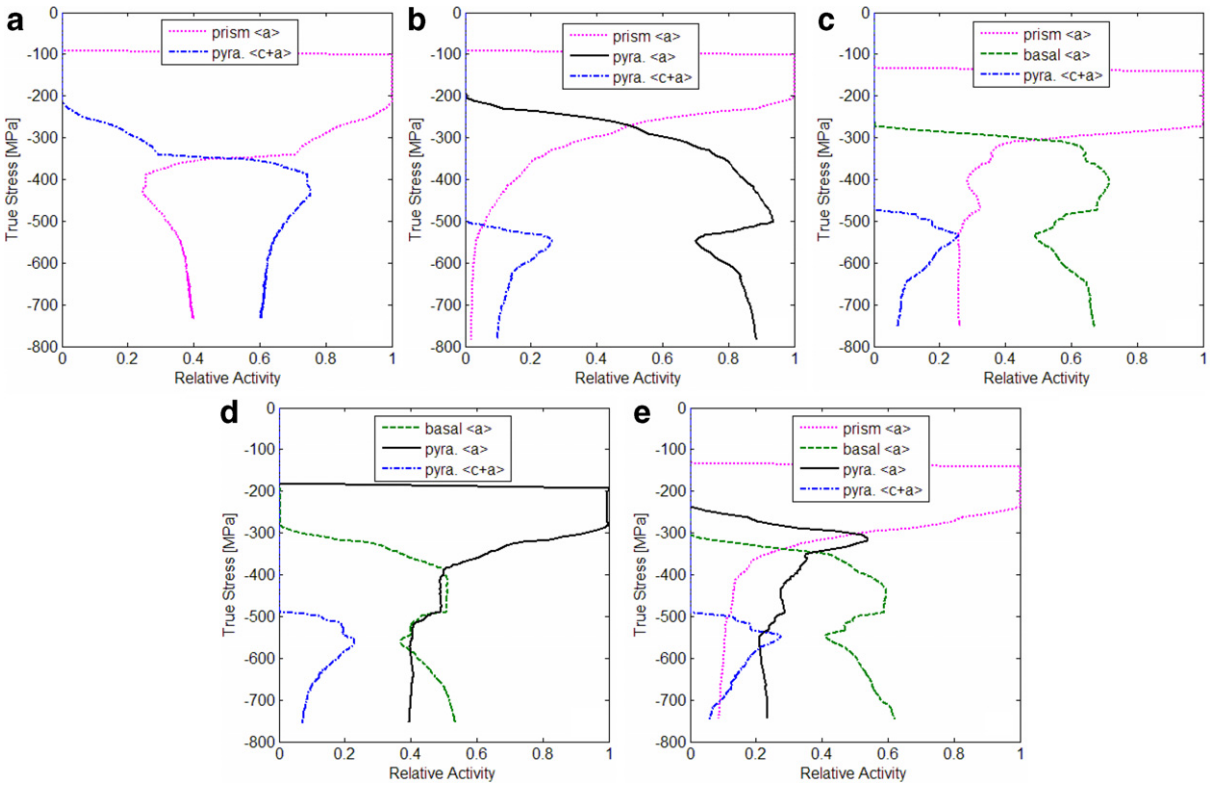

Fig. 7. Relative activities of slip systems as a function of applied true stress: (a) Case I, (b) Case II, (c) Case III, (d) Case IV and (e) Case V.

pyramidal $\langle a\rangle$-slip in Case IV) initiates first, followed by basal or pyramidal $\langle a\rangle$-slip, and then by pyramidal $\langle c+a\rangle$-slip. This corresponds to the sequence of micro-yielding in the prism, the lower-order pyramidal, the higher-order pyramidal, and the basal orientations. It appears that the micro-yielding of the basal orientation (or the initiation of pyramidal $\langle c+a\rangle$-slip) is responsible for the macroscopic yielding of the material. This is clear when comparing the evolution of relative activities (Fig. 7) and the corresponding flow curves (Fig. 1).

The relative activity of pyramidal $\langle c+a\rangle$-slip develops in a similar pattern in Fig. 7(c) (Case III) and Fig. 7(d) (Case IV). This happens to basal slip as well, but with lower activity in Case IV, because in Case IV its role has been partially assumed by pyramidal $\langle a\rangle$-slip.

Fig. 7(c) and (e) reveal a close similarity in the activity of pyramidal $\langle c+a\rangle$-slip between Cases III (Fig. 7(c)) and V (Fig. 7(e)). More interestingly, the total amount of relative activities of prism slip and pyramidal $\langle a\rangle$-slip in Case V is commensurate with the activity of prism slip in Case III. Basal slip is roughly the same active in both cases, although part of its role in Case III may have been taken by pyramidal $\langle a\rangle$-slip in Case V. In other words, pyramidal $\langle a\rangle$-slip can be assumed as a combination of prism and basal slip.

5. Discussion

5.1. Effects of twinning

Even a small volume fraction of twins, of either tensile or compressive types, can bring about remarkable stress relaxation in the $\{0002\}$ orientation [32]. To maintain stress equilibrium as well as strain compatibility, orientations other than $\{0002\}$ would also experience changes in their internal stress state, but the resultant effects are largely dependent on the volume of twins. Twins can also affect the subsequent plastic deformation after their formation, by facilitating or impeding the movement of dislocations. In this paper, we deliberately ignore twinning modes in the modeling in order to avoid another level of complexity. Since twinning is not likely to occur significantly in these specimens, because of its low Schmid factor, it will not contribute significantly to the results reported here. Specifically, the validity of disregarding twinning modes in Comp.ND is justified by the following:

(1) TEM experiments have shown no tension or compression twins of any type in the specimens compressed along ND [35].
(2) Texture measurements and intensity analyses suggested that the texture changes little during compression along ND [33]. If twinning activity was significant, the texture and intensities would have changed dramatically.

5.2. Reasonable ranges of CRSS

Reasonable CRSSs of the deformation systems should meet the following requirements:

(1) Reproduce macroscopic flow curves for Comp.ND, Tens.TD and Tens.RD.
(2) Predict Lankford coefficients for the above-mentioned three deformation conditions.
(3) Predict the relative activity of prism slip (except for Case IV), i.e. prism slip should be the most active system in any conditions, at least during the early stage of plastic deformation.
(4) Capture the main features of the lattice strain development (at least in the loading direction for some cases) during Comp.ND, i.e. the micro-yielding orientations should follow a sequence of the prism initially, then the pyramidal, and the basal finally.

Being tested against the above constraints, the wide ranges of initial CRSSs given in Section 3 have been dramatically narrowed down to those listed in Table 4, and the best sets for each case are tabulated in Table 2.

5.3. Separation of $\{10\bar{1}1\}$ and $\{10\bar{1}2\}$ lattice strains

In Ref. [32], we speculated that the failure to separate predicted $\{10\bar{1}1\}$ and $\{10\bar{1}2\}$ lattice strains in the loading direction during Comp.ND resulted from the omission of pyramidal $\langle a\rangle$-slip in the modeling. In this paper, we have shown that the separation is present not only in Case II (with pyramidal $\langle a\rangle$, Fig. 3), but also in Case I (without pyramidal $\langle a\rangle$, Fig. 2). Further studies have shown that even in Case III ('pr+bas+pyca'), it was possible to separate lattice strains of the two pyramidal peaks. Fig. 8 shows an example of the separation, with initial CRSSs being $\tau_0^{pr}=0.11$ GPa, $\tau_0^{bas}=0.34$ GPa and $\tau_0^{pyca}=0.24$ GPa. Thus we may deduce that this separation can be fulfilled either by other slip systems (e.g. pyramidal $\langle c+a\rangle$-slip) than pyramidal $\langle a\rangle$-slip, or by pyramidal $\langle a\rangle$-slip only, which probably has been practically represented by others in modeling.

Table 4
Reasonable ranges of initial CRSSs ([min, max] in GPa)

	Case I	Case II	Case III	Case IV	Case V
Prism $\langle a\rangle$-slip	[0.08, 0.11]	[0.08, 0.10]	[0.09, 0.11]	–	[0.09, 0.10]
Basal $\langle a\rangle$-slip	–	–	[0.14, 0.17]	[0.14, 0.18]	[0.16, 0.18]
Pyr. $\langle a\rangle$-slip	–	[0.11, 0.13]	–	[0.11, 0.13]	[0.14, 0.16]
Pyr. $\langle c+a\rangle$-slip	[0.14, 0.19]	[0.28, 0.32]	[0.32, 0.36]	[0.34, 0.36]	[0.30, 0.33]

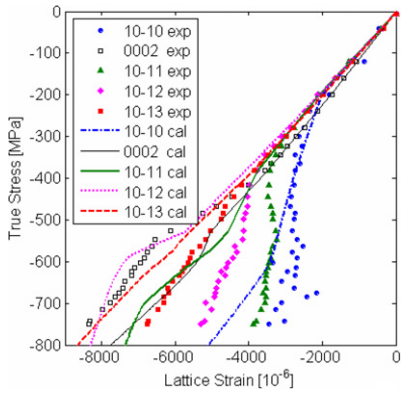

Fig. 8. Separation of $\{10\bar{1}1\}$ and $\{10\bar{1}2\}$ lattice strains using prism, basal and pyramidal $\langle c+a\rangle$-slip.

5.4. Possibility of pyramidal $\langle a\rangle$-slip

In the published papers (e.g. [15,23,24]) which do not consider basal slip, the deformation (tension or compression) typically proceeds in the direction along which only a few high-order pyramidal or basal grains are orientated. This probably explains why their modeling results are reasonable even without basal slip, since low-order pyramidal orientations present small Schmid factors for basal slip, but large factors for pyramidal $\langle a\rangle$-slip.

It would be difficult to prove the necessity of including pyramidal $\langle a\rangle$-slip using the current EPSC model and our present experimental lattice strain data (due to the notable texture changes in the cases other than Comp.ND). The fact that satisfactory agreement of the model with experimental results can be obtained without pyramidal $\langle a\rangle$-slip and the complete absence of evidence that it exists in Zr and its alloys suggests that one should be extremely cautious about introducing pyramidal $\langle a\rangle$-slip into any model.

6. Conclusion

We have illustrated the necessity of including basal slip in the EPSC modeling of the room-temperature deformation in polycrystalline Zircaloy-2 by considering extensive combinations of slip systems. Based on the fitting to our neutron diffraction data, we believe that (1) basal slip is very active during plastic deformation, and should be considered in the EPSC modeling; (2) pyramidal $\langle a\rangle$-slip can reasonably be neglected, especially if one wants to simplify the modeling process by using fewer modeling parameters and that (3) a combination of prism slip, basal slip and pyramidal $\langle c+a\rangle$-slip is the smallest set of deformation systems necessary for modeling. We have also proposed reasonable ranges of initial CRSS for each slip system, which can serve as reference starting values for the EPSC modeling of Zr alloys with similar chemical compositions.

Acknowledgement

The authors thank Dr C.N. Tomé of Los Alamos National Laboratory for his assistance in the modeling work. Feng Xu also thanks Mr M. Kerr of Nuclear Group at Queen's University in Canada for helpful discussions. This work is sponsored by NSERC, COG, OPG and Nu-Tech Precision Metals under the Industrial Research Chair program in Nuclear Materials at Queen's University.

References

[1] R.G. Ballinger, G.E. Lucas, R.M. Pelloux, J. Nucl. Mater. 126 (1984) 53.
[2] R.W. Cahn, Acta Metall. 1 (1953) 49.
[3] E.J. Rapperport, Acta Metall. 3 (1955) 208.
[4] E.J. Rapperport, Acta Metall. 7 (1959) 254.
[5] J.E. Bailey, J. Nucl. Mater. 7 (1962) 300.
[6] A. Akhtar, J. Nucl. Mater. 47 (1973) 79.
[7] J.A. Jensen, W.A. Backofen, Can. Met. Quart. 11 (1972) 39.
[8] E. Tenckhoff, Z. Metallkd. 63 (1972) 192.
[9] D.H. Baldwin, R.E. Reed-Hill, Trans. AIME 233 (1965) 248.
[10] R.E. Reed-Hill, in: R.E. Reed-Hill, J.P. Hirth, H.C. Rogers (Eds.), Deformation Twinning, AIME, 1964, p. 295.
[11] J.I. Dickson, G.B. Craig, J. Nucl. Mater. 40 (1971) 346.
[12] A. Akhtar, Acta Metall. 21 (1973) 1.
[13] K. Pettersson, J. Nucl. Mater. 105 (1982) 341.
[14] J.L. Martin, R.E. Reed-Hill, Trans. TMS AIME 230 (1964) 780.
[15] M.J. Philippe, C. Esling, B. Hocheid, Texture. Microstruct. 7 (1988) 265.
[16] P.A. Turner, C.N. Tomé, Acta Metall. 42 (1994) 4143.
[17] R.A. Lebensohn, C.N. Tomé, Acta Metall. Mater. 41 (1993) 2611.
[18] J.W.L. Pang, T.M. Holden, P.A. Turner, T.E. Mason, Acta Mater. 47 (1999) 373.
[19] H. Francillette, B. Bacroix, M. Gaspérini, J.L. Béchade, Mater. Sci. Eng. A 234–236 (1997) 974.
[20] H. Francillette, B. Bacroix, M. Gaspérini, J.L. Béchade, Acta Mater. 46 (1998) 4131.
[21] H. Francillette, O. Castelnau, B. Bacroix, J.L. Béchade, Mater. Sci. Forum 273–275 (1998) 523.
[22] C.N. Tomé, private communication, 2006.
[23] M.J. Philippe, F. Wagner, C. Esling, in: J.S. Kallend, G. Gottstein (Eds.), Proceedings of the 8th International Conference on Textures of Material (ICOTOM-8), The Metallurgical Society, 1988, p. 837.
[24] C.N. Tomé, R.A. Lebensohn, U.F. Kocks, Acta Metall. Mater. 39 (1991) 2667.
[25] S.R. Agnew, D.W. Brown, C.N. Tomé, Acta Mater. 54 (2006) 4841.
[26] F. Xu, R.A. Holt, M.R. Daymond, R.B. Rogge, E.C. Oliver, Mater. Sci. Eng. A (submitted for publication).
[27] M.R. Daymond, H.G. Priesmeyer, Acta Mater. 50 (2002) 1613.
[28] B. Clausen, T. Lorentzen, M.A.M. Bourke, M.R. Daymond, Mater. Sci. Eng. 259 (1999) 17.
[29] J.R. Cho, D. Dye, K.T. Conlon, M.R. Daymond, R.C. Reed, Acta Mater. 50 (2002) 4847.
[30] P.A. Turner, N. Christodoulou, C.N. Tomé, Int. J. Plasticity 11 (1995) 251.
[31] C.N. Tomé, G.R. Canova, U.F. Kocks, N. Christodoulou, J.J. Jonas, Acta Metall. 32 (1984) 1637.
[32] F. Xu, R.A. Holt, M.R. Daymond, Acta Mater (submitted for publication).
[33] F. Xu, R.A. Holt, M.R. Daymond, R.B. Rogge (in preparation).
[34] R.A. Holt, D. Dye, R.B. Rogge, Annual Report of the National Research Council, 2004.
[35] I. Yakubtsov, private communication, 2006.